Asteroid modeling for testing spacecraft approach and landing

Martin, Iain; Parkes, Steve; Dunstan, Martin; Rowell, Nick

Published in:
IEEE Computer Graphics and Applications

DOI:
10.1109/MCG.2014.22

Publication date:
2014

Document Version
Peer reviewed version

Asteroid Modeling for Testing Spacecraft Approach and Landing

Iain Martin, Steve. Parkes, *Member, IEEE*, Martin Dunstan and Nick Rowell

***Abstract*— Spacecraft exploration of asteroids presents a variety of autonomous navigation challenges that can be aided by virtual models to test and develop guidance and hazard avoidance systems. This paper describes the extension and application of graphics techniques to create high-resolution, virtual asteroid models to simulate cameras and other spacecraft sensors approaching and descending towards asteroids. A scalable model structure with evenly spaced vertices is specified to simplify terrain modeling, avoid distortion at the poles and enable triangle strip definition for efficient rendering. The base asteroid models are created using both a two-phase Poisson faulting technique and Perlin noise. Realistic asteroid surfaces are created by adding synthetic crater models adapted from lunar terrain simulation and multi-resolution boulders to the base models. The synthetic asteroids are evaluated by comparison with real asteroid images, slope distributions, and by applying a surface relative feature tracking algorithm to the models.**

***Index Terms*— terrain modeling, fractal, terrain relative navigation, vision guidance.**

I. Introduction

Asteroids are a sub-class of small solar system bodies that orbit the Sun and are usually rocky or metallic with most orbiting in the region between Mars and Jupiter. They can vary widely in form but most that have been observed are rough, irregularly shaped objects. Asteroids larger than around 300 km in diameter such as Vesta and Ceres are roughly spherical but smaller asteroids are irregularly shaped because their mass is too small to force a spherical shape through gravity.

A. Asteroid Form

On rocky, solid planetary bodies with no atmosphere, impact cratering is generally the dominant geological process with the Moon, Mercury and most asteroids having heavily cratered surfaces. The surface of the Moon contains many similarities to the surfaces of asteroids and in particular the forms of craters and the saturated cratered surfaces are similar because impact craters have a similar profile on all rocky planetary bodies with some variance due to surface density and gravitational strength [1].

Manuscript received MON-DD-YYYY; revised MON-DD-YYYY. This work was supported in part by European Space Agency Contracts; Asteroid and Whole Planet study (ESA Contract No. (17338/03/NL/LVH/BJ) and Asteroid Extension Contract No. (20858/07/NL/EK)

I. Martin, S. Parkes, M. Dunstan and N. Rowell are at the Space Technology Centre, University of Dundee, UK e-mail: imartin@computing.dundee.ac.uk

Asteroid Spacecraft Landers

To approach and land on an asteroid, a spacecraft needs to navigate to the asteroid, adjust its velocity to match the asteroid tumbling or enter an orbit, navigate to the target landing site and descend to the surface avoiding hazards. For some near-Earth asteroids it may be possible to control a spacecraft from Earth but autonomous spacecraft control is required to land on further away objects because of the signal time-delay.

Autonomous vision and LIDAR[1] (Light Detection And Ranging) based systems are being developed to provide technology to land safely on the surface of the Moon, Mars and other solid bodies. LIDAR is an optical remote sensing laser that can scan the distance to a target.

For example, the Hayabusa asteroid lander used both vision and LIDAR to approach asteroid Itokawa[2] and the current European Space Agency's Lunar Lander program[3] proposes a combined vision and LIDAR based autonomous landing system.

It is difficult to create physical simulations to test and develop an asteroid approach and lander so there is a requirement for synthetic models to provide simulated camera and LIDAR images to test autonomous guidance and hazard avoidance systems.

[1] J. de Lafontaine, D. Neveu, and J. Hamel, "Autonomous planetary landing using a LIDAR sensor: the Landing Dynamic Test Facility", In Proc. ESA Conference on Guidance Navigation & Control Systems (GNC), 2008.

[2] T. Kubota, T. Hashimoto, S. Sawai, J. Kawaguchi, K. Ninomiya, M. Uo, and K. Baba, "An Autonomous Navigation and Guidance System for MUSES-C Asteroid Landing", Acta-Astronautica, 52(2), 2003.

[3] R. Fisackerly, J. Carpenter, D. De Rosa, A. Pradier, C. Philippe, and B.Gardini and "The European Lunar Lander: Robotic Operations in a Harsh

Craters are classified as simple or complex, with simple craters having bowl shaped interiors with intact rims and craters larger than the simple to complex transition diameter (related to the mass and surface density of the planetary body) having flatter bottoms, collapsed rims and may have central uplift. Simple craters formed from recent impacts tend to have sharp well defined rims and bowl shaped interiors but over long periods of time degrade into shallower depressions [1]. Crater diameter distributions, rim heights and diameter/depth ratios can vary on different asteroids.

Figure 1 shows images of four asteroids with differing morphological characteristics and a comparison between a surface image of Vesta and a synthetic lunar surface [2] to highlight the similarities.

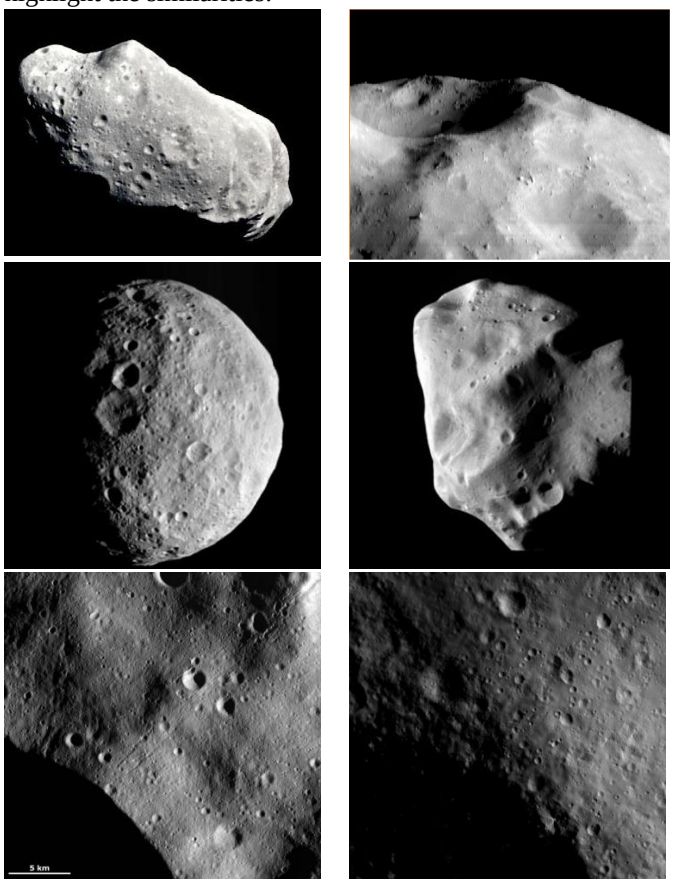

Figure 1: NASA Galileo image of Ida (top left), NEAR Shoemaker image of the surface of Eros (top right), Dawn image of Vesta (center left), Rosetta image of Lutetia (center right), surface image of Vesta (bottom left) and synthetic lunar cratered terrain (bottom right).

Previous research has simulated the surface of the Moon, Mars and Mercury for testing planetary landers [2] and this paper extends that research to model asteroids by applying and adapting graphical techniques to create rough asteroid shaped objects and then adding synthetic crater and boulder models in realistic distributions. It is important to have a high-resolution model to obtain consistency between the rendered images from multiple sensors (e.g. LIDAR as well as vision) and for an accurate ground truth to calibrate the tests. Rendering images to simulate vision-based navigation may not require the same frame rate as smooth animation so although fast rendering is desirable it is not as critical as realistic simulation of crater-saturated asteroid surfaces. The speed of terrain modelling is also of secondary importance because models can be generated off-line before running simulations.

II. RELATED WORK

Three dimensional models of many asteroids have been generated from Earth-based time-resolved photometry but their resolution is too low for testing navigation and landing systems although potentially they could be used as base models on which to add further high-resolution artificial terrain. There is a 1 m per pixel model of Asteroid Itokawa generated from the extensive imaging taken by the orbiting Japanese Hayabusa spacecraft but this method of creating models is limited to asteroids visited by modern spacecraft and the Itokawa model is not representative of larger asteroids with cratered surfaces.

Gaskell describes the creation of synthetic asteroid models for navigation approach and landing [3] where low-resolution asteroid shape models are extended by random additions and the addition of fresh craters and protruding mounds to simulate boulders. The shape models created are realistic but the craters are clearly all fresh and do not simulate the cratered surfaces of most asteroid with craters in varying stages of degradation. There is little detail given on the creation of the asteroid mesh structure, however the approach of adding craters and boulders to asteroid shape models creates the most realistic models in the published work in this field.

Fractal techniques can be used to generate realistic, artificial rocky terrain. The most widely used are derived from the model of fractional Brownian motion such as Random Mid-point Displacement (RMD), fractional noise and Poisson faulting. RMD can be applied to a general mesh object through triangle subdivision but the fractal objects generated are faceted and in our results were more applicable to simulating boulders than asteroids.

A variety of fractal planets have been generated by Poisson faulting [4] and by summing different frequencies of noise functions such as Perlin or Simplex noise [5]. For example, Esbert describes a general approach to simulate terrain and planets with procedural techniques and noise functions [6] and Compton describes an implementation of Perlin noise to generate random planetoids [7]. While these implementations produce detailed planets with varying fractal terrain they do not realistically model most asteroids because they do not simulate crater saturated surfaces. However, they could be used to generate base models on which realistic crater models could be added or for simulating small rubble-pile asteroids such as Itokawa. Other related terrain modeling techniques focusing on simulating Earth-like terrain (e.g. ridges and valleys) or filling gaps in elevation models with Gaussian process modeling are not directly suitable for modeling asteroids because they also don't generate cratered terrain with overlapping craters.

Texturing can add surface detail to mesh models to give the impression of higher resolution without increasing the mesh

resolution but can be problematic with issues such as repeated patterns which could be picked up by image-processing algorithms and difficulties with the large resolution ranges required to simulate an asteroid approach and descent. Normal mapping perturbs surface normals to simulate surface detail but does not alter the underlying geometry so would be unrealistic at the silhouette (edge of the rendered model) and also add complexity to dynamic shadow generation.

A combination of surface parameterization [8] and displacement maps [9] may improve the rendering performance of terrain maps in general but this approach was not implemented in this work because simulation realism was prioritized over rendering speed. However, it may be reasonable to improve rendering performance by deriving low-resolution parameterized surfaces and displacement maps from high-resolution asteroid models if accompanying tessellation techniques are used to recreate the resolution of the model geometry when rendering.

This paper applies and adapts prior work in this area to create asteroid models for testing small body approach and landing systems by the creation of a scalable model that avoids polar distortion, applying fractal terrain modeling algorithms to create a base asteroid shape and adding realistic craters and boulders to the shape models to simulate realistic asteroid surfaces. High-resolution polygon meshes are then generated to create an asteroid model representation that can be rendered to simulate both vision and LIDAR sensors from the same data source.

III. ASTEROID MESH STRUCTURE

The model mesh structure is a critical component for both terrain modeling and efficient rendering. The primary requirements for our mesh model are to enable efficient selection of neighboring vertices in all directions to support resolution scalable terrain modeling algorithms and to have similar distances between vertices throughout for even rendering. A secondary requirement is for a mesh structure suitable for efficient rendering.

A spherical mesh structure was chosen to model the asteroids because a deformed spherical model could represent the wide variety of asteroid forms from lumpy misshapen objects to near-spherical planetoids. Cube decomposition is an alternative structure which would also be reasonable. A widely used spherical mesh structure is to define strips of polygons along latitudes with a triangle fan at the poles. This structure was not used because the size of the polygons varies from larger around the equator to small thin triangles at the poles which can cause distortion and over-rendering effects of flickering pixels in high-resolution models. These effects could be reduced by generic level-of-detail rendering algorithms but also by defining a mesh structure with evenly sized polygons at the expense of a more complex mesh structure.

Our solution is to define evenly spaced vertices in a latitude/longitude data structure for terrain modeling so that neighboring vertices can be efficiently obtained for adding surface features such as craters or boulders and then convert to triangle strips of vertices for efficient rendering through recursive sub-division of triangle strips for efficient view-culling. Figure 2 shows the difference between a spherical mesh structure with evenly spaced vertices and the structure with thin triangles at the poles.

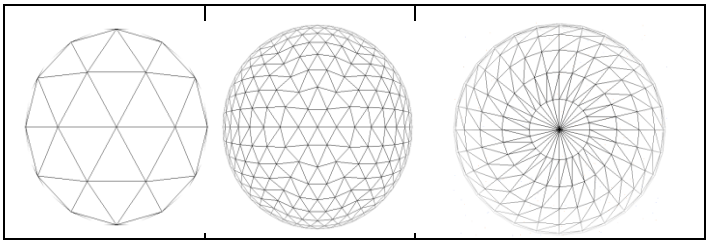

Figure 2: View of a pole from the evenly spaced mesh structure (left and center) and the uneven structure with a triangle fan at each pole (right).

A. *Modeling mesh structure*

The asteroid model data structure is defined as an array of height points in latitude longitude coordinates. Magnitude M defines the number of rings of latitude in each hemisphere, including the equator but ignoring the poles giving the number of mesh vertices as $6M^2+2$. There are $6L$ vertices in latitude ring L where L=1 corresponds to the latitude ring closest to the pole and latitude ring M corresponds to the equator which is shared by the two hemispheres creating a scalable mesh with an near-evenly spaced structure throughout as shown in Figure 3.

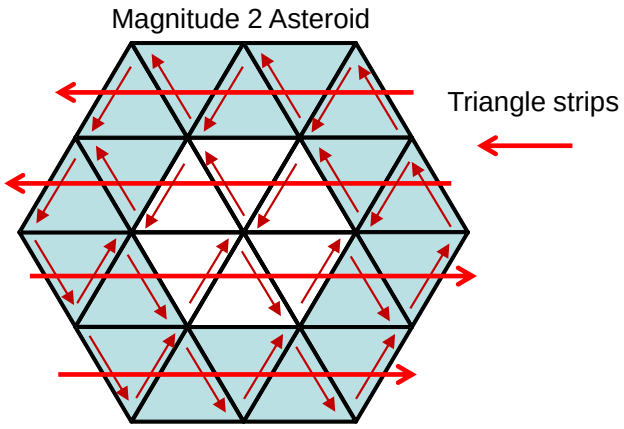

Figure 3: The mesh structure of the Northern hemisphere of a magnitude 2 asteroid model with four triangle strips defined.

B. *Rendering mesh structure*

To enable efficient rendering of asteroid models, the latitude/longitude data structure has to be converted into an efficient polygon structure in a resolution scalable algorithm. There are a variety of generic polygon meshing techniques which could be used in place of our method so we just give an overview of our technique which was optimized for our rendering system.

To avoid problems such as an unrealistically low-resolution silhouette and additional complexity for both dynamic shadow casting and LIDAR renderings, the mesh model is defined at the same resolution as the latitude/longitude data structure defining the asteroid surface. LIDAR instruments can be

simulated by calculating the intersection of the LIDAR beam with the model geometry to obtain the distance from the instrument to the surface at the LIDAR beam position and direction. A displacement map does contain the necessary surface detail to calculate this but additional processing would be required to calculate the correct intersection point to the displacement map as the LIDAR beam could be at any angle or orientation to the displacement map.

We generate long triangle strips across the model as shown in Figure 3 and then recursively sub-divide the strips improve view-culling which is a standard technique to improve rendering speed of large models where only triangle strips visible from the current view position are rendered. Large triangle strips limit view culling because if even a small part of one strip is visible in the field of view, the rendering system must render the entire strip. This is appropriate for simulating asteroids because at least half of the asteroid will always be out of view.

For typical asteroids with magnitudes of 500 or more the meshes produced have tens of thousands of strips with several thousand vertices in each strip. We recursively subdivide the triangle strips to produce a tree with small triangle strip meshes at the leaves with a parameter, *K*, specifying the desired number of strips and strip size within mesh patches. If the current mesh contains at least *K* strips and the longest strip contains at least *K* triangles then the mesh will be split into four by dividing into two groups of strips and splitting each strip in half. The resulting meshes are further subdivided until they reach the requested size which is set to optimize performance on specific hardware.

IV. Modeling Asteroid Form

We use both a variant of Poisson faulting and Perlin noise to generate realistic base asteroid models from the flexible mesh structure because the two techniques produced comparable results.

A. Two Phase Poisson Faulting Asteroids

Poisson faulting can be applied to a sphere to add surface roughness [4]. A single fault is applied by choosing a great circle at random which splits the sphere into two hemispheres. All height points on one hemisphere are modified by a fault height calculated from a Gaussian random distribution scaled by the maximum fault size. The great circle is selected by defining a vector with a random direction which defines the normal to a plane intersecting the origin splitting the sphere in two equal parts as shown in Figure 4 (top row). The sign of the dot product between each vertex point and the random vector determines in which hemisphere each vertex lies, providing an efficient method to apply faults which is important because Poisson faulting is a slow $O(N^3)$ algorithm. A fractal surface is obtained by applying a large number of small faults. The surface roughness can be controlled by the maximum fault size and the number of faults and can be stretched along one axis to create an elongated shape, but the overall form does not model the irregular lumpy form of most asteroids because Poisson faulting creates surfaces which tend to a fractal dimension of 2.5 which makes it difficult to create surfaces with the required range of roughness.

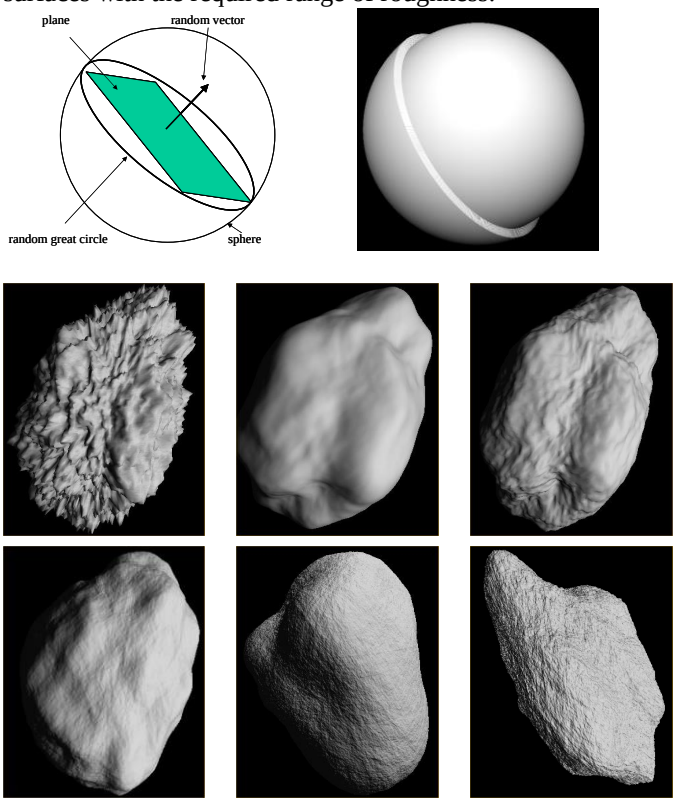

Figure 4: Poisson faulting: defining a random great circle (top left) and the result of applying a fault (top right), the three stages of the Poisson faulting technique (middle row) and three asteroid models (bottom row).

The general form of many asteroids can be simulated by a two phase Poisson faulting method creating different frequencies of roughness. An excessively rough object is created with Poisson faulting using a large maximum fault size. A smoothing filter is applied followed by a second phase of Poisson faulting with a small maximum fault size. The smoothing filter has the effect of removing high frequency terrain leaving an undulating surface. Surface roughness is then added by a second phase of Poisson faulting. The three stages of this process are Figure 4 (middle row) with the left image showing a 100 m stretched model after applying 1000 faults with maximum size of 5 m. The central image shows the smoothed model and the right image shows the model after the second phase of Poisson faulting of 500 faults with a maximum size of 0.5 m. Varying the number of faults in each phase and the width and number of smoothing filter passes generates a wide variety of different asteroid models.

B. Perlin Noise Asteroids

Coherent noise functions (e.g. Perlin or Simplex) are widely used in graphics for adding realism to many types of simulations. A one-dimensional Perlin noise function can be created by defining pseudo-random gradient vectors spaced along a line. A continuous function is created by interpolating with a blending function such as $f(t) = 3t^2 - 2t^3$, or

$f(t) = 6t^5 - 15t^4 + 10t^3$ [7]. Fractional Brownian noise can be created by summing noise functions of increasingly higher frequency and lower amplitude and can be extended to *n* dimensions to generate artificial rocky terrain models. Standard parameters that control the form of terrain generated are the number of summed noise functions (octaves), the frequency of the lowest frequency band (frequency), the amplitude drop with frequency band (persistence) and the frequency multiplier between successive bands (lacunarity). Further control can be obtained by customizing the frequency and amplitude changes between specific frequency bands.

A three-dimensional Perlin noise function with ten octaves was implemented and sampled on the surface of a normalized sphere to obtain displacement values for a magnitude 400 asteroid. Three sets of noise parameters were used to create different asteroid base models as shown in Figure 5.

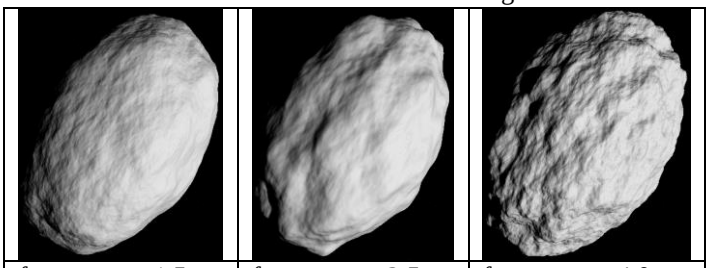

frequency = 1.5 persistence = 0.5 lacunarity = 1.75	frequency = 2.5 persistence = 0.5 lacunarity = 1.5	frequency = 4.0 persistence = 0.3 lacunarity = 2.5

Figure 5: Perlin noise asteroid models with varying standard noise parameters.

Coherent noise functions can be considered superior to Poisson faulting for generating base asteroid models because they are inherently more flexible and considerably faster. However, the implementation of Poisson faulting in different phases had good results so is also presented and model generation speed isn't a critical issue because the models can be generated offline.

V. Adding Craters to the Asteroid

The literature on asteroid craters shows that their form is similar to lunar craters but they may have different rim heights, depth/diameter ratios and diameter distributions. It is therefore reasonable to adapt a previously developed lunar crater model to apply to asteroid surfaces. This crater model is described in previous research [7] so we give only an overview of the model characteristics to describe the asteroid specific adaptations. This crater model is designed to apply to a two-dimensional Digital Elevation Model (DEM) so we have adapted it to apply to asteroid objects. Crater profiles are defined by smoothly connected polynomials parameterized by crater diameter, depth, rim height and age. Fresh craters have sharp, well defined rims but degrade over long time periods with decreasing rim height and a shallower bowl as shown in Figure 6. Craters have a similar profile with some random variances because the energy of crater-forming impacts is such that the angle of incidence of the object doesn't affect the form of the crater produced except for rare, extremely low-angled impacts [1].

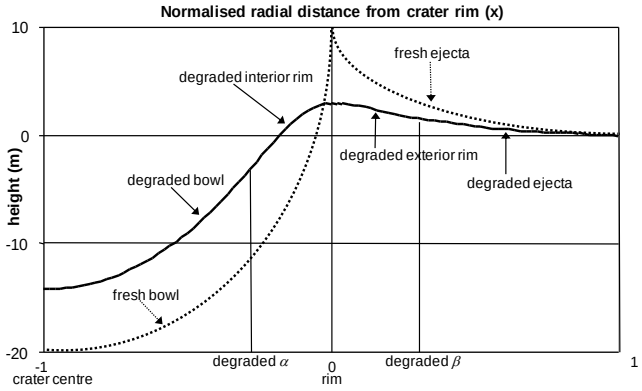

Figure 6: Fresh and degraded crater profiles [3].

Fresh crater rim height and depth are related to crater diameter [1]. The normalized erosional state of a crater is calculated by extrapolating the degradation profile defined for of a crater of a specific diameter, to craters of all diameters. The crater model is smoothly integrated into rough terrain by replacing the underlying crater bowl region with a plane representing the surface slope before adding the crater bowl to the plane and then merging the ejecta into the surrounding terrain. A high-frequency fractal overlay, parameterized by radial distance from the crater center, is generated and added to the crater region to add surface roughness to the new bowl region and to add additional roughness to the ejecta. This crater model can be added to slopes and overlap other craters so that crater saturated surfaces can be modeled by impacting large numbers of craters with the appropriate diameter and age distributions to suit the specific planetary body.

A. Crater Addition Algorithm

To add craters to an asteroid, a two dimensional data structure is first constructed storing the height value, angle and distance from the crater center for each latitude/longitude point in the impact region. The horizontal resolution of the DEM is defined to match the average distance between vertex points in the asteroid.

All vertices in the crater region are selected and added to a list, storing terrain height, angle and distance to the crater center. The latitude/longitude data structure simplifies the task of defining a crater addition region because neighboring vertices can be easily found along the current and latitudes until out of range and similarly along latitudes north and south until no vertices are in range. The angle between each vertex and the crater center is calculated using the cosine rule and a reference normal to determine whether the angle is obtuse or acute. To map vertices to the DEM, vectors directly east and north from the crater center are defined and scaled to the distance between two vertices on the current latitude. DEM coordinates are calculated from the dot products of each vertex and the east and north vectors. Any holes in the grid are filled by interpolating neighboring points using a weighted average of the nearest known values in eight directions. The crater model is then added to the DEM using the actual distances and angles between the vertex points instead of grid distances for

crater model calculations. The crater region is mapped back to the asteroid model, by first storing the new height value in the latitude/longitude array and then calculating the difference in heights between the asteroid point and the corresponding grid point. We then rescale the length of the vector defining the vertex point by the height difference.

A general issue associated with mapping an area of curved surface both to and from a DEM is that numerical approximations or inaccuracies can result in radial artifacts. In this instance, artifacts are introduced if the distance and angle are calculated from the mapped positions in the DEM instead of using vertex distances. Artifacts can also be introduced around crater rims when craters are added to excessively steep slopes. These artifacts can be eliminated or reduced by adding in a slope based erosion factor which reduces crater depth and rim height on steep slopes. We can justify eroding craters on steep slopes because this happens in reality with surface creep due to gravity. Limiting the large asteroid impacts can be justified by the fact that really large impacts may destroy the asteroid and the lumpy shape model is simulating the effects of ancient, large impacts

B. *Generating crater lists*

To create a cratered asteroid model we generate lists of crater definitions specified by position, diameter and age. To obtain an even distribution of crater positions around a sphere, a vector is defined from three random numbers and normalized.

(1) $v_r(x,y,z) = (r_1, r_2, r_3), r_i \in [-0.5, 0.5], v_r \neq (0,0,0)$

(2) $v_n = \frac{V_r}{|V_r|} = \left(\frac{r_1}{l}, \frac{r_2}{l}, \frac{r_3}{l}\right), l = \sqrt{({r_1}^2 + {r_2}^2 + {r_3}^2)}$

The normalized vector, v_n, is then converted into latitude and longitude as follows:

(3) $lat = sin^{-1}(v_n(y))$

(4) $\begin{cases} lon = cos^{-1}\left(\frac{v_n(x)}{\cos(\text{lat})}\right), \text{if } v_n(z) \geq 0 \\ lon = 2\pi - cos^{-1}\left(\frac{v_n(x)}{\cos(\text{lat})}\right), \text{if } v_n(z) < 0 \end{cases}$

Realistic crater diameter distributions can be obtained by implementing distributions defined in the literature for different areas of the Moon [1] and some well-studied asteroids. Crater diameter distributions are commonly specified as cumulative size-frequency distributions defining $N_{cum}(D)$ as the number of craters per unit area greater than a given diameter D. This can be closely approximated by $N_{cum}=cD^k$ where k is approximately −1.8 for lunar mare surfaces and when k=-2, N_{cum} is dimensionless so the crater population appears the same at all resolutions. The number of craters (per unit area) within a specific diameter range can then be calculated as:

(5) $N(D_{min}, D_{max}) = N_{cum}(D_{min}) - N_{cum}(D_{max})$

The constant c can be calculated when the range of crater diameters is defined and the cumulative frequency values for the range of crater diameters are known [1].

C. *Boulder modeling*

The surface of most asteroids visited by spacecraft have been found to contain a variety of boulders (e.g. asteroid Eros shown in Figure 1) and were implemented by Gaskell in prior work on asteroid modeling [3] so a boulder model was implemented to simulate the surfaces of some asteroids.

A multi-resolution mesh based on a regular icosahedron was developed to procedurally create boulders from a small set of initial parameters that control the general form and roughness characteristics. Boulders are created with multiple levels of detail so that the most appropriate level can be selected for rendering at runtime to avoid over rendering artifacts. Higher resolutions are obtained through RMD triangle edge subdivision by inserting new vertices between existing vertices and new strips between existing strips.

Multi-resolution boulders are represented as a sequence of bi-resolution nodes as shown in Figure 7 which represents a 4-level boulder generated starting at level *B*. The low-resolution branch of the first node holds the mesh of the lowest-resolution *B* while the high-resolution branch holds the node for all the higher resolution meshes. This is repeated until the bottom level is reached which has mesh level *B*+2 in the low-resolution branch and level *B*+3 in the high-resolution branch. The rendering system can select the most appropriate mesh to render based on the distance from the camera and mesh screen size. Figure 7 shows the base boulder mesh as a flattened icosahedron, the bi-resolution mesh structure and example synthetic boulders.

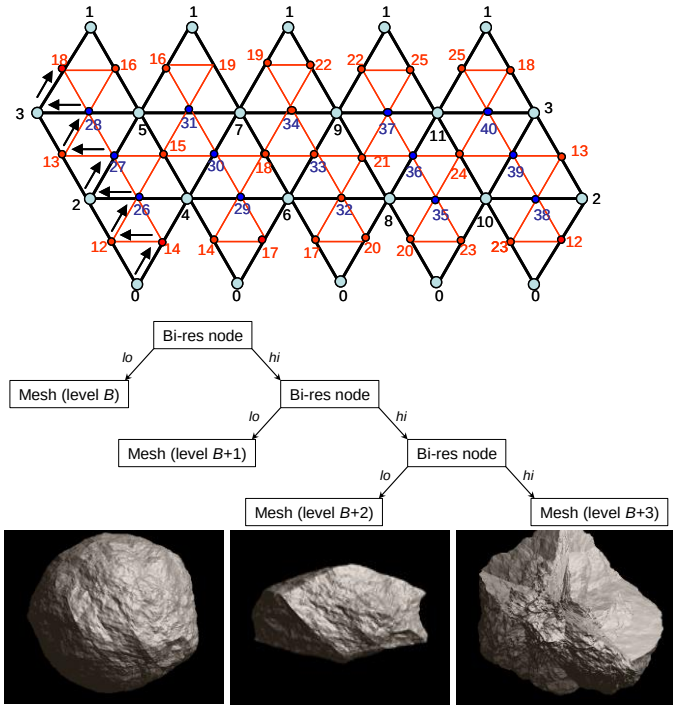

Figure 7: Multi-resolution boulder generation based on an icosahedron

Boulder lists for asteroids are created using the same technique as for craters with size and burial depth obtained from distributions. Placing boulders onto an asteroid surface is more complicated than adding them to a flat or curved DEM-based model. Each boulder is initially rotated so that the "up" axis is aligned with the local zenith axis i.e. a boulder at the north pole has no rotation while one at the equator will be

rotated by 90° and one at the south pole by 180°. For consistency, boulders are also rotated about their local vertical axis to account for the longitude of the boulder. The 3D position on the surface is computed and then adjusted to take burial depth into account. The boulder can then be randomly rotated around each local axis.

VI. Results and Evaluation

This section shows the results of the asteroid modeling by displaying rendered images and LIDAR simulations from asteroids models, evaluating slope distributions and by comparing the results of applying a feature tracking system to real images and synthetic models. The images were generated using a custom OpenGL based renderer without applying surface textures so that both LIDAR and standard images could be rendered at the same resolution.

A. Examples of asteroid models

Figure 8 (top left) shows a rendered from a noise based asteroid models with a crater diameter distribution of $N_{cum}=0.5D^{-2}$ and top right from a Poisson faulting based model with a crater distribution of $N_{cum}=0.1D^{-2}$. The middle row shows false color representations of two LIDAR images approaching an asteroid with the distance to the target shown by a range of colors with red representing nearest to the sensor. The simulated LIDAR images can be used identify hazards such as steep slopes and boulders by an autonomous landing system.

Figure 8 (bottom) shows a sequence of images approaching a magnitude *M=1000* asteroid with the five lowest resolution asteroids rendered as imposters showing that the modeling and rendering techniques can provide the range of images to simulate a spacecraft approaching an asteroid. The imposter is created by rendering the model at full size to a texture which is applied to a correctly scaled, camera facing quad (a billboard).

B. Slope Distribution

To evaluate the realism of the asteroid models, slope distributions were compared with a 3° resolution slope area histogram of Asteroid Eros from data collected by the Laser Rangefinder instrument on the NEAR-Shoemaker space craft [11]. A variety of models were constructed to generate a range of asteroid types with slope distributions plotted against the Eros data.

Two magnitude *M=400* base asteroid models were created, one with a Poisson faulting base and the other with a summed Perlin noise base, to determine if the slope distribution of the artificial models could be representative of a real asteroid. By trial and error, the Poisson faulted model parameters used were 1000 faults up to 5 m, three smoothing passes with 20 m filters, a second phase of faulting with 20000 faults up to 0.03 m, a factor 2 stretch on the x axis and a crater diameter distribution of $N_{cum}=0.5D^{-2}$. The Poisson faulting parameters given in Figure 5 were used for this experiment.

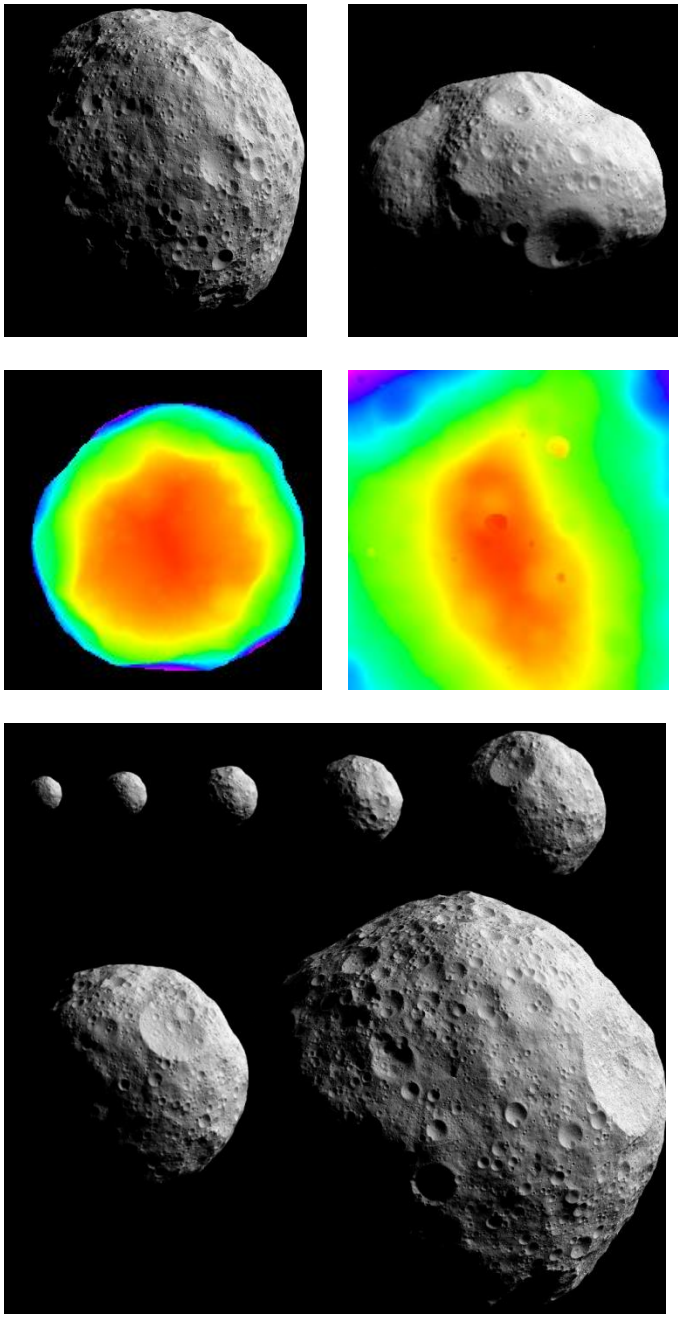

Figure 8: Perlin noise based asteroid model (top left), a stretched Poisson faulting base asteroid model (top right), two images from a LIDAR scan simulation (middle) and a sequence of images approaching an asteroid model with approximately six million vertices.

Slope values were calculated for all vertex points using a weighted slope average of all vertices within a 3° radius and were collated into cumulative slope frequency values from which the slope area histogram was calculated as shown in Figure 9 (top) which demonstrates that both the spherical and stretched versions of the model have reasonably similar slope distributions to Eros. Plots are also given of rougher models with double the amount of craters, and rougher Poisson faulting to demonstrate how these parameters affect slope distribution. A similar plot is given for the three Perlin

asteroid based models specified Figure 5 (left, middle and right) with the same crater distribution ($N_{cum}=0.5D^{-2}$) added to compare the slope characteristics obtained.

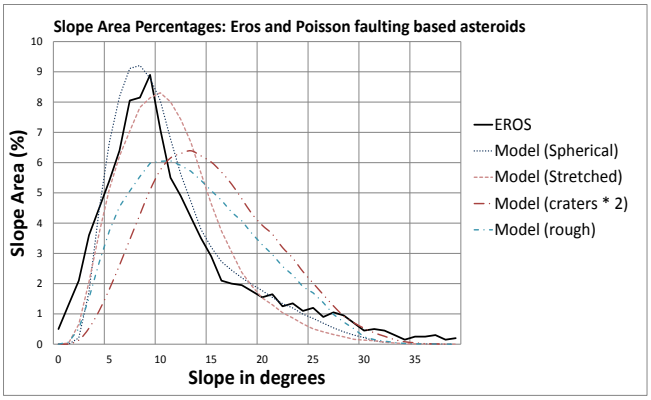

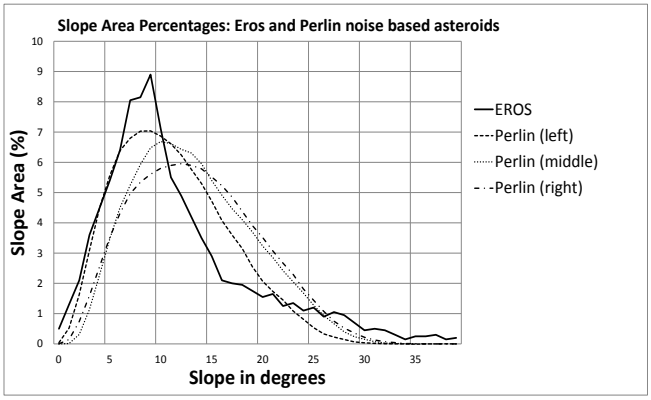

Figure 9: Slope area histogram comparisons of asteroid Eros [11]and Poisson faulting based artificial models (top) and the three noise based models as defined in Figure 5 (bottom).

C. *Feature Tracking*

Feature tracking is widely used in vision-based navigation and guidance systems where feature points are identified and tracked across a sequence of images with the motion of these tracks used for a variety of optical navigation algorithms. For example, approximately seven tracks are sufficient to reproduce the motion of the spacecraft in relation to the surface. To evaluate the response of the models to a realistic image processing navigation scenario, a feature tracking algorithm [12] based on the Harris corner detector was applied to image sequences approaching synthetic asteroid models

Three image sequences are shown pictorially in Figure 10 where the lines represent feature points tracked across multiple images in the motion sequence. The top left image shows a tumbling synthetic asteroid and a stationary camera position, the top right image shows an approach towards another tumbling synthetic asteroid. The tracks show that sufficient features can be tracked on a spinning model with a moving spacecraft. The bottom right image shows feature points extracted from a real image of asteroid Lutetia and the bottom left a corresponding set of features extracted from a synthetic asteroid. We can see that in both the real image and the images rendered from the virtual models that a reasonable spread of feature points are selected and if tracked could be used by an autonomous navigation system to determine the motion of the spacecraft with respect to the asteroid. The Itokawa model was not used for comparison with our models because the small, rubble asteroid is different to the larger cratered asteroids on which our synthetic models were based.

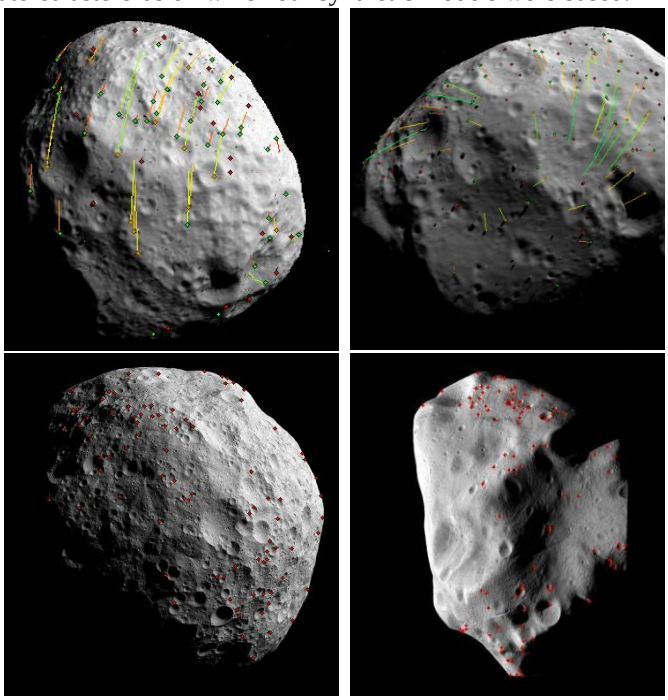

Figure 10: Feature point selection algorithm applied to images from: mid-resolution Poisson faulting based asteroid models (top left and top right), high-resolution Perlin noise based asteroid (bottom left) and a single image of Lutetia from ESA's Rossetta mission (bottom right).

VII. Conclusions

We have described the application and extension of terrain modeling algorithms to simulate irregular asteroid shapes for testing spacecraft navigation and approach. The scalable mesh structure aids the application of terrain modeling algorithms, avoids polar distortion, and using the isometric canonical coordinate system, provides a logical and efficient technique to define triangle strips that can then be recursively subdivided for rendering optimization.

Noise functions are a more efficient and controllable technique to generate asteroid base models than Poisson faulting. However, although the multi-phase faulting technique does not generate asteroid models to a particular form to simulate a specific asteroid, it can generate a wide variety of realistic asteroid shapes and could also be used to add detail to low-resolution asteroid base models. We also more closely approximated the slope characteristics of Eros using the two-phase Poisson faulting technique than the noise models although a similar match for a noise based asteroid could probably have been created through further control of the noise parameters. The Poisson faulting parameters are simpler (two fault size, and the smoothing filter size) and create realistic base models but the slow algorithm does not scale well taking considerable time to generate high-resolution

models.

The adaptation of the previously developed lunar crater model generates crater saturated asteroid surfaces that can be tailored to a particular surface type by applying the appropriate diameter and age distributions. The limitations identified with the mapping technique are that large craters extending greater than approximately 60° of the asteroid radius can have artifacts near the edge of their ejecta and craters on steep local slopes can also have artifacts. These problems can be avoided by limiting the maximum angular extent of craters and by eroding craters on steep slopes which may unduly affect the slope characteristics of the model by reducing the number of larger impacts.

Multi-resolution boulders and imposters enable the rendering of high-resolution models at a wide range of distances avoiding over-rendering artifacts. The LIDAR simulations demonstrate the suitability of generating high-resolution models from which multiple sensors can be simulated without the use of textures which may not be applicable to all simulated sensors.

The slope profile of a range of models was compared to the slope profile of asteroid Eros and shown that asteroid models can be created with a realistic slope profile but also that a range of slope profiles can be generated by modifying the asteroid base model parameters and by the distribution of craters added. Additionally, the application of a vision guidance feature tracking algorithm shows that the synthetic asteroid images behave similarly to real images when this algorithm is applied.

We conclude that the application and adaption of graphical and terrain modeling techniques presented could be used to create a range of high-resolution asteroid models for testing and developing future autonomous asteroid navigation and guidance systems.

VIII. Future Work

The current system is not suitable for generating models of asteroids such as Mathilde that are dominated by excessively large craters with diameter near the mean radius of the asteroid. Modifications to the crater model are required to model this scenario realistically. Research into characterizing noise functions to model specific asteroid forms may be useful for generating models for specific mission scenarios, e.g. to generate models with a defined range of slope characteristics but would also have to take into account the slope contribution of the cratering.

To improve the realism of the asteroid images, the reflectance models used could be enhanced to match the spectral characteristics of different asteroid types. Rendering performance may be enhanced with displacement maps and tessellation shaders if the resulting images are of the same quality as the high-resolution mesh approach and LIDAR can be accurately simulated.

IX. Acknowledgment

The authors would like to acknowledge the support of the European Space Agency for the work described in this paper, in particular ESA project managers Olivier Dubois-Matra, Salvatore Mancuso and Stein Strandmoe. Some of the work described in this paper was partly funded by ESA Contract No. 20858/07/NL/EK led by the University of Dundee.

X. References

[1] H. Melosh, *Impact Cratering – A Geologic Process*, Oxford University Press, 1989.

[2] S. Parkes, M. Dunstan, I. Martin, M. McCrum and O. Dubois-Matra, "Testing Advanced Navigation Systems for Planetery Landers and Rovers," in *In Proceedings of the 60th International Astronautical Congress*, Daejeon, Republic of Korea, Oct. 2009.

[3] R. Gaskell, "Small body simulations for navigation approach and landing", *AIAA Space Conference and Exposition*, vol. 3, 2005, pp. 1613–1620.

[4] B. Mandelbrot, *The Fractal Geometry of Nature*, New York: WH Freeman & Co., 1988.

[5] A. Lagae, S. Lefebvre, R. Cook, T. DeRose, G. Drettakis, D. Ebert, J. Lewis, K. Perlin, M. Zwicker, "A survey of procedural noise functions", *Computer Graphics Forum* 29, 8 (December 2010), 2579–2600.

[6] D. Esbert, F. Musgrave, D. Peachey, K. Perlin, S. Worley, *Texturing & Modelling A Procedural Approach*, Third Edition, Morgan Kaufmann, 2003.

[7] K. Compton, J. Grieve, E. Goldman, O. Quigley, C. Stratton, E. Todd, A. Willmott, "Creating Spherical Worlds", *SIGGRAPH 2007*, ACM, New York, NY, USA, Article 82.

[8] N. Pietroni, M. Tarini, P. Cignoni, "Almost isometric mesh parameterization through abstract domains", *IEEE Trans. on Visualization and Computer Graphics*, Volume 16, 2010.

[9] L. Szirmay-Kalos, T. Umenhoffer, "Displacement mapping on the GPU – state of the art", *Computer Graphics Forum*, 2008.

[10] I. Martin, S. Parkes, M. Dunstan, "Modeling Planetary Surfaces with Real and Synthetic Terrain", *IEEE Trans. Aerospace and Electronic Systems, to be published*.

[11] M. Zuber, D. Smith, A. Cheng, et al., "The Shape of 433 Eros from the NEAR-Shoemaker Laser Rangefinder", *Science*, Vol. 289, No. 5487., 2097-2101 , 2000.

[12] N. Rowell, S. Parkes, M. Dunstan, "Image processing for near Earth object based vision guidance system", *IEEE Trans. on Aerospace and Electronic Systems*, vol.49, no.2, 2013.

Iain Martin Dr. Iain Martin is a lecturer at the Space Technology Centre at the University of Dundee. His research interests include planet surface simulation for autonomous spacecraft, testing of vision based guidance systems, 3D graphics and SpaceWire networks.

Steve Parkes Prof. Steve Parkes is a Chair of Spacecraft Electronic Systems and director of the Space Technology Centre, School of Computing, University of Dundee, Scotland. Professor Parkes leads research work on the design and development of spacecraft on-board data-handling networks (SpaceWire), planet surface simulation and autonomous lander navigation, and digital signal and image processing for satellites. Professor Parkes is a member of the IEEE.

Martin Dunstan Dr. Martin Dunstan is a postdoctoral research fellow working on the visualization of simulated planet surfaces and spacecraft using OpenGL GNC landing and orbital rendezvous maneuvers.